Advances in Energy and Materials Research https://jaem.qom.ac.ir/

Influence of dispersion interactions on the adsorption of NTCDA on Ag(110)

Alireza Abbasi ✉1 | Michael Schreiber 2 | Reinhard Scholz 3

1. Correspond author, Department of Chemistry, Faculty of Science, University of Qom, Qom, Iran. E-Mail: a.abbasi@qom.ac.ir
2. Institut für Physik, Technische Universität Chemnitz, D-09107 Chemnitz, Germany. E-Mail: schreiber@physik.tu-chemnitz.de
3. Leibniz Institut für Polymerforschung, Hohe Straße 6, 01069 Dresden, Germany. E-Mail: scholz@ipfdd.de

Article Info

Article type:
Research Article

Article history:
Received 30 June 2023
Received in revised form 12 July 2023
Accepted 1 August 2023
Published online 9 October 2023

Keywords:

ABSTRACT

In the present work, the adsorption of 1,4,5,8-naphthalene tetracarboxylic dianhydride (NTCDA) on a (110)-oriented silver substrate is investigated with second-order Møller-Plesset perturbation theory (MP2). The metal surface was modeled using rigid silver clusters of finite size, allowing to test of the convergence of the optimized adsorbate geometry as a function of the size of the metal cluster. The geometry is converged for most of the substrate models, but the adsorption energy depends more severely on the size of the metal cluster. The dispersion interaction included in MP2 gives a nearly flat adsorbate geometry, whereas its lack of density functional theory (DFT) results in a bent geometry arising from strong silver-oxygen interactions and overlap repulsion in the central part of the molecule. Irrespective of the method used, the carboxylic oxygens interact more strongly with the substrate than the anhydride oxygen atoms, so that their height above the topmost substrate layer is significantly smaller. On the largest silver clusters used, MP2 converges to a height of 2.57 Å for the carbon atoms, somewhat closer than a value of 2.68 Å obtained with MP2 for the similar but larger molecule PTCDA on the same substrate orientation.

Cite this article: Abbasi, A. Schreiber, M. & Scholz, R. (2023). Influence of dispersion interactions on the adsorption of NTCDA on Ag(110), *Advances in Energy and Materials Research*, 1 (1), 12-22. https://doi.org/10.22091/JAEM.2023.9638.1004

Publisher: University of Qom.
DOI: https://doi.org/10.22091/JAEM.2023.9638.1004

1. Introduction

During the last decades, several studies have focused on organic semiconductors due to their potentially interesting properties for electronic and optoelectronic applications, including organic light emitting diodes (OLEDs) [1,2], organic field effect transistors (OFETs) [3,4] and organic solar cells [5]. The performance of such devices is determined by the transport properties of the organic material and by the interface with the contacting material. Hence, the interaction between the metal contact and the molecules adsorbed at the metal-organic interface plays a key role in the entire device [6-9]. The net charge of the adsorbate multiplied by the distance between the adsorbate and the topmost metal layer may contribute to a substantial interface dipole, modifying in turn the alignment between the frontier orbitals of the molecule and the Fermi energy in the contact. Therefore, a precise knowledge of the adsorbate geometry becomes mandatory for a quantitative understanding of the energetic alignment of transport levels at the interface required for efficient injection or extraction of charges.

For a few molecule-metal interfaces, normal-incidence X-ray standing-wave (XSW) techniques have been used to obtain precise information concerning the height of the adsorbed species to the topmost substrate layer, including reference cases like PTCDA (3,4,9,10-perylene tetracarboxylic dianhydride) [10-13] deposited on Ag(111) and Ag (110) [13-16], and NTCDA (1,4,5,8- naphthalene tetracarboxylic dianhydride) [17] deposited on Ag(111). Both compounds form closed monolayers with the molecular plane oriented parallel to the substrate surface. These good con- trolled adsorbate structures reveal interesting microscopic information, including the activation energy for thermal desorption [18], tunneling spectra, and shifts of the core levels to thicker polycrystalline films [10, 19-22]. XSW measurements of NTCDA on Ag(111) have demonstrated that the carboxylic oxygens are closer to the substrate than the aromatic core, indicating the formation of rather strong chemical bonds between the functional groups and the substrate [17]. Possible height modulations within the carbon backbone are more difficult to track so the evaluation of the experimental data remains restricted to an average height, where a reduced coherent fraction represents destructive interference of C atoms placed at different distances from the topmost substrate layer [17]. In a first attempt, DFT calculations seemed to reproduce the XSW geometry obtained for PTCDA on Ag(111) [23], but in a revised calculation with more extended variational orbitals, a much too shallow potential minimum occurred at an adsorbate-substrate distance of about 0.5 Å above the experimentally determined height [24,25]. An analysis of the density-density response function constructed within the random phase approximation on top of a DFT calculation provides the dispersion interaction required for an interaction potential resembling the experimental situation [26]. This work demonstrates that DFT based on the local density approximation (LDA) results in a substantial overbinding, with an interaction potential resembling erroneously a realistic dispersion interaction, whereas functionals employing the well-tested generalized gradient approximation (GGA) underestimate the adsorption energy. Hybrid functionals like B3LYP cannot cure this deficiency because both the underlying GGA functional and the Hartree-Fock part result in similar failures of the interaction potential.

An alternative computational approach to dispersion interactions arises naturally from post-Hartree-Fock methods, including configuration interaction (CI) or coupled cluster (CC) schemes. As these approaches scale very steeply with the system size, they can only be applied to rather small systems, including, e.g., pairs of small aromatic molecules like benzene, naphthalene, or anthracene [27-32].

Second-order Møller-Plesset perturbation theory (MP2) still keeps track of the leading order of the van-der-Waals attraction arising from double excitations, and to the more advanced schemes, its scaling with the fifth power of the system size N remains moderate. Therefore, for very small systems, its range of applicability can be tested against more expensive methods like CC techniques including single and double excitations together with a perturbative treatment of triple excitations (CCSD(T)) scaling as N^7 [27, 28, 32] For rather large systems, MP2 emerges as a suitable compromise including the main part of the dispersion interactions at affordable cost. However, due to the scaling of N^5, calculations close to the basis set limit cannot be performed for large chemisorbed molecules, so the numerical results need to be corrected for a substantial basis set superposition error (BSSE). It has been shown analytically that the Boys-Bernardi counterpoise (CP) scheme is an adequate method for treating the BSSE in a full CI calculation [33, 34]. Hence, the BSSE-CP method remains a valid approximation of CI restricted to double excitations, and MP2 contains the second-order perturbation term of the total ground state energy arising from these double excitations. In that respect, it was found that the MP2 procedure combined with medium-size basis sets can provide accurate reaction energies and relaxed complex geometries [35, 36], and for systems dominated by dispersion interactions, BSSE-CP corrected interaction potentials can dramatically improve the convergence with the size of the basis set.

In the present work, we apply MP2 and the B3LYP hybrid functional to an investigation of the adsorption geometry of NTCDA on the Ag(110) surface. Figure 1 shows the molecular structure and two frontier orbitals of the NTCDA molecule. The rather open (110)-oriented silver surface was chosen because it is known that the adsorbate unit cells of both, NTCDA and PTCDA, contain only a single molecule, indicating that the adsorbate-substrate interaction is much stronger than intermolecular interactions in the adsorbate layer. Moreover, for NTCDA, previous DFT studies have already determined the preferential adsorption site, allowing it to handle all numerical calculations within the adsorbate point group C_{2v} [37]. The rather large intermolecular distances between adjacent chemisorbed NTCDA molecules underpin the fact that they interact only via electric multipoles.

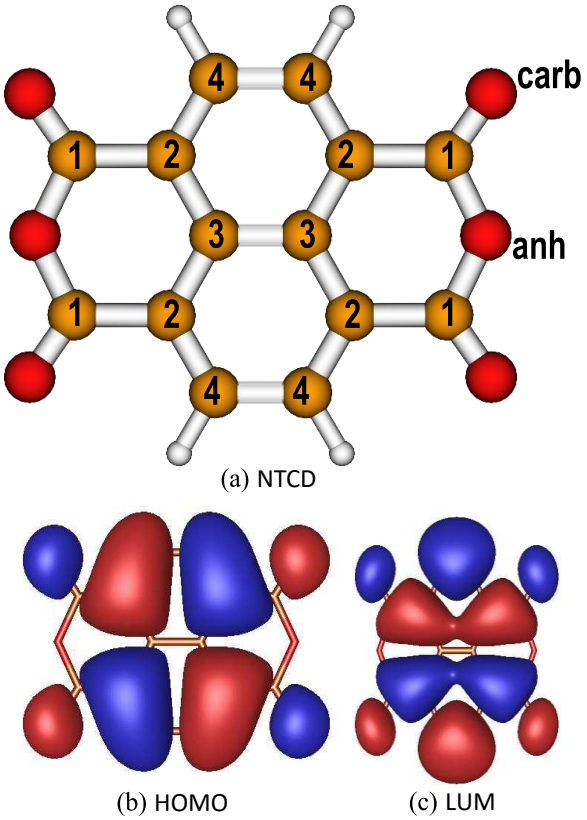

Figure 11. (a) Molecular structure of NTCDA. Each index addresses atoms in equivalent positions.

MP2 versus B3LYP

In the present study, we have applied MP2 using the resolution-of-identity approximation for the evaluation of two-electron integrals (RIMP2) [38], as implemented in the TURBOMOLE software package [39]. For comparison with a method excluding dispersion interactions, we have applied DFT using the hybrid functional B3LYP with an exchange-correlation energy calculated on an integration grid of medium density (m4).

Silver was treated with an effective core potential based on 28 core electrons, accounting for scalar relativistic effects (ECP-28-MWB [40]). A def-SV(P) basis set [41] was chosen for the atoms in NTCDA. This basis set was selected because we have previously shown [42, 43] that an MP2 calculation of the organic adsorbate PTCDA on a noble metal performed in a similar SV(P) basis generates already a small overbinding, a phenomenon expected for a sufficiently large variational basis set due to an overestimation of the entire dispersion interaction at the MP2 level. The calculated adsorbate geometry was very close to a subsequent determination of the adsorption height with normal incidence XSW experiments [13, 44].

To obtain the relaxed structure of NTCDA adsorbed on the Ag(110) surface, we start from a geometry in keeping with the known adsorption site derived from DFT calculations [37]. Since the positions of the silver atoms on the metal surface are not expected to change strongly due to the interaction with the adsorbate, it is convenient to fix the position of all silver atoms during the geometry optimization of the adsorbate.

Substrate models

For periodic adsorbate structures, one common choice of substrate consists of several atomic layers within a supercell, but for non-local exchange and long-range dispersion interactions, the infinite extension of the periodic system becomes challenging. Alternatively, an aperiodic metal cluster of sufficient size can be used, so that the mathematical problems arising from periodicity are exchanged against an unavoidable influence of the cluster size on the computed results. As the long-range correlation included at the MP2 level is difficult to investigate for a periodic system, except molecular crystals with relatively small dispersion interactions [45-47], for our system a cluster model of the substrate emerges as the only possible choice. For selected systems, the use of a finite approximant for the substrate may even give better results than a periodic calculation.

In the present work, five different silver clusters were used to model the Ag(110) surface (Figure 2). The smallest cluster has 9 atoms in the first layer, corresponding exactly to the unit cell required by chemisorbed NTCDA on Ag(110), and 4 and 3 atoms in the second and third layers, respectively, altogether 16 silver atoms which are denoted as Ag_{16}(9,4,3). To speed up the calculations, we investigate only Ag(110) clusters with C_{2v} symmetry, coinciding with the largest point group a D_{2h}-symmetric molecule can realize as an adsorbate.

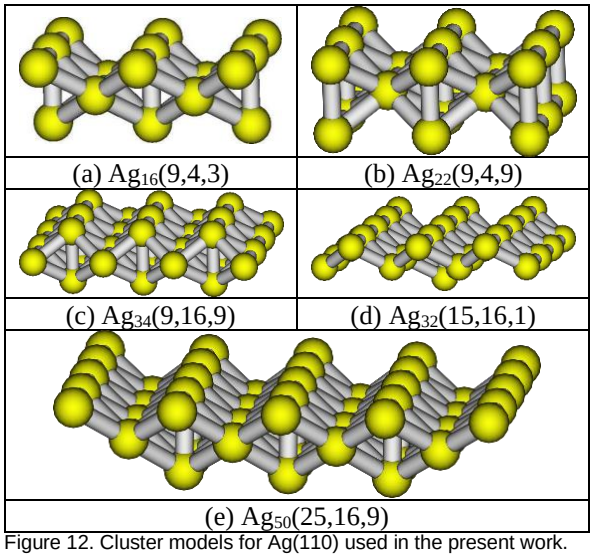

Figure 12. Cluster models for Ag(110) used in the present work.

Results

In the TURBOMOLE 5.7 code used, the optimization is still subject to the BSSE. As the distance between the adsorbate and substrate is the most important configuration coordinate, we have used the optimized adsorbate geometry and scanned the interaction energy along the distance between the adsorbate and substrate cluster. By applying the Boys-Bernardi CP scheme [48], such a scan reveals the influence of the BSSE on the interaction potential. For all substrate clusters, the BSSE-CP scheme reduces the adsorption energy substantially. Moreover, the distance dependences of the raw data including the BSSE and the BSSE-CP corrected potential energy surfaces (PESs) differ, so that the position of the energetic minimum of the BSSE-CP corrected PES is shifted to a larger distance. As an example, Figure 3 visualizes the PES of the interaction between NTCDA and an $Ag_{22}(9, 4, 9)$ substrate cluster obtained at the MP2/def-SV(P) level. The CP correction of the BSSE produces a substantial reduction of the adsorption energy and the minimum of the CP PES shifts by 0.18 Å to a larger distance from the substrate.

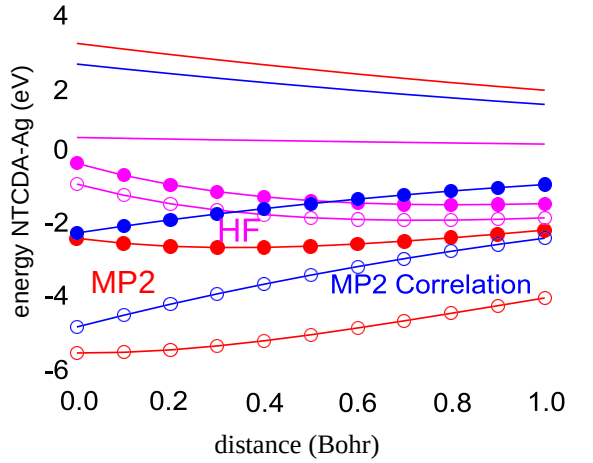

Figure 3. MP2/def-SV(P) adsorption energy of NTCDA on $Ag_{22}(9,4,9)$ along the distance between molecule and substrate, compared to the geometry optimized without correction of the BSSE. •: with BSSE-CP correction,[33] ○: without; lines without symbols: the size of BSSE correction for the different energetic contributions (magenta: Hartree-Fock, blue: correlation at the MP2 level, red: MP2).

Table 6. Height differences (Å) between selected atoms in the adsorbate. □O is the difference between the heights of the anhydride and carboxylic oxygens, and □C1 is the difference between a carbon atom in one of the end groups and the average over the naphthalene core. The bending along the long axis is defined as □long = zC3 − zC1, and the lateral bending as □short = zC3 − zC4. For a periodic calculation with the PBE functional, it was found that the Ag atoms below the carboxylic

[a] Calculation using the B3LYP hybrid plus pairwise dispersion interactions [49].

[b] Calculation using a periodic supercell and the PBE functional [37].

cluster	z_C	$z_{C(core)}$	z_{C1}	z_{C2}	z_{C3}	z_{C4}	z_O	$z_{O(carb)}$	$z_{O(anh)}$	z_H	E_{ads}	Δz
MP2											−1.00	
$Ag_{16}(9,4,3)$	2.63	2.64	2.59	2.64	2.64	2.65	2.52	2.50	2.57	2.79	−2.44	0.14
$Ag_{22}(9,4,9)$	2.65	2.65	2.64	2.70	2.68	2.58	2.53	2.48	2.64	2.70		0.18
$Ag_{32}(15,16,1)$	2.60	2.62	2.56	2.64	2.61	2.60	2.46	2.42	2.55	2.72	−1.52	0.16
$Ag_{34}(9,16,9)$	2.57	2.57	2.56	2.63	2.58	2.51	2.45	2.39	2.57	2.62		0.16
											−0.45	
B3LYP											0.13	
$Ag_{16}(9,4,3)$	3.96	3.99	3.90	3.97	3.97	4.01	3.86	3.86	3.87	4.02	−0.35	0.03
$Ag_{22}(9,4,9)$	2.91	2.96	2.78	2.98	3.04	2.91	2.60	2.53	2.74	2.90		0.06
$Ag_{32}(15,16,1)$	2.81	2.88	2.65	2.87	2.93	2.86	2.45	2.40	2.57	2.89	−0.29	0.04
$Ag_{34}(9,16,9)$	2.88	2.94	2.74	2.97	3.03	2.87	2.54	2.46	2.71	2.86	−0.52	0.08
$Ag_{50}(25,16,9)$	2.95	3.01	2.79	3.03	3.10	2.95	2.59	2.52	2.74	2.90		0.11
											0.05	
B3LYP+D3[a]												
$Ag_{32}(15,16,1)$	2.74	2.80	2.61	2.80	2.86	2.77	2.43	2.38	2.54	2.78	−2.27	0.04
PBE[b]		2.62					2.43	2.40	2.50	2.62	−0.92	

Table 7. Height differences (Å) between selected atoms in the adsorbate. □O is the difference between the heights of the anhydride and carboxylic oxygens, and □C1 is the difference between a carbon atom in one of the end groups and the average over the naphthalene core. The bending along the long axis is defined as □long = zC3 − zC1, and the lateral bending as □short = zC3 − zC4. For a periodic calculation with the PBE functional, it was found that the Ag atoms below the carboxylic atoms are raised out of the topmost substrate plane [37], a phenomenon ignored in our approach based on rigid substrate clusters (last column).

cluster	δ_O	δ_{C1}	δ_{long}	δ_{short}	δ_{Ag}
MP2		−0.04		−0.01	
$Ag_{16}(9,4,3)$	0.07	0.00	0.04	0.09	–
$Ag_{22}(9,4,9)$	0.16	−0.04	0.03	0.01	–
$Ag_{32}(15,16,1)$	0.14	−0.01	0.05	0.07	–
$Ag_{34}(9,16,9)$	0.18		0.03		–
B3LYP		−0.06		−0.04	
$Ag_{16}(9,4,3)$	0.00	−0.13	0.07	0.13	–
$Ag_{22}(9,4,9)$	0.21	−0.17	0.26	0.07	–
$Ag_{32}(15,16,1)$	0.17	−0.14	0.28	0.15	–
$Ag_{34}(9,16,9)$	0.25	−0.16	0.29	0.15	–
$Ag_{50}(15,16,9)$	0.22		0.31		–
PBE	0.10				0.07

Effect of cluster size on the adsorption geometry

For several substrate clusters, Figure 4 represents the optimized geometries and Table 1 summarizes the heights of different atoms in NTCDA to the topmost silver layer. The distances were obtained from the minimum of the BSSE-CP corrected PES, occurring typically at about 0.14 to 0.18 Å larger distances compared to the optimized RIMP2 geometries without BSSE- CP correction. During this scan, all internal geometry parameters of the adsorbate were kept fixed. In the B3LYP calculation, the BSSE is rather small, so

the distance shifts obtained from the BSSE-CP corrected potential minimum remain below 0.1 Å for most substrate models. Table 2 relates this height information to internal deformations of the adsorbate to a planar NTCDA molecule.

Irrespective of the computational scheme and cluster size, the two types of oxygen atoms occur at different heights. The height distortion δ_O gives a direct measure of the different strengths of the respective interactions with the substrate. Except for the smallest substrate cluster $Ag_{16}(9,4,3)$ where the silver sites below the carboxylic oxygen are rather far from the coordination in an extended topmost monolayer (ML), the distortion δ_O has similar values on all larger model clusters. In principle, this height difference is accessible to XSW measurements, as demonstrated for PTCDA and NTCDA on Ag(111) and Ag(110) substrates [10, 11, 13, 17, 23, 44].

Other height distortions in the adsorbate are less pronounced. For all substrate clusters, the strong attraction between oxygen atoms and substrate bends the carbon atoms C1 between the oxygen atoms downwards to the core region of the adsorbate. The overlap repulsion between the peripheral C4-H region and the substrate increases significantly for the cluster $Ag_{32}(15,16,1)$ with the largest lateral extension, resulting in an essentially flat naphthalene core with particularly small lateral deformation δ_{short}. This indicates that the somewhat larger lateral distortions δ_{short} occurring on the substrate models $Ag_{22}(9,4,9)$ and $Ag_{34}(9,16,9)$ are merely artifacts resulting from a too-small extension of each of these clusters along the respective direction, reducing, in turn, the attractive dispersion interaction.

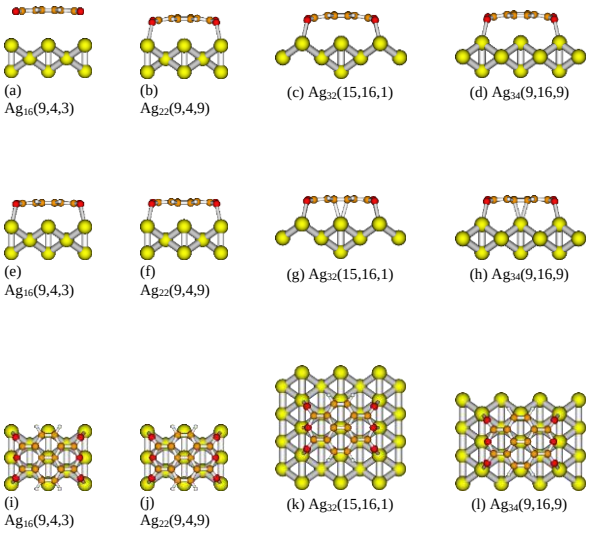

Figure 13. Optimized geometries of NTCDA on different cluster models of Ag(110) surface. Top row: B3LYP geometries. Second row: MP2 geometries. Third row: Top views of MP2 geometries. Fourth row: B3LYP geometry of NTCDA on Ag50(25,16,9): m) side view and n) top v

Due to computational limitations arising from the steep scaling of MP2 with system size, in none of our substrate clusters, all 9 surface atoms in direct contact with the adsorbate could be surrounded by all 7 nearest neighbors occurring in an extended topmost ML. As indicated in Figure 2, this would require an $Ag_{50}(25,16,9)$ model cluster. The best compromise seems to be the $Ag_{34}(9,16,9)$ cluster, realizing 7 nearest neighbors for the central site in the topmost ML and 6 nearest neighbors for the surrounding topmost Ag atoms. Hence, we expect the respective adsorbate geometry to be the most reliable for the majority of sites, except C4 and H where the distortion δ_{short} should be best represented by the substrate model $Ag_{32}(15,16,1)$ with the largest lateral extension. Moreover, both for the substrate models $Ag_{34}(9,16,9)$ and $Ag_{32}(15,16,1)$, the large number of silver atoms in the second layer has a significant impact on the total amount of attractive dispersion interaction, so both of these substrate models result in a reduced distance between adsorbate and metal surface.

Impact of van der Waals (vdW) interaction on adsorption geometry

The DFT calculations performed with the B3LYP hybrid do not contain any partial compensation between overlap repulsion and dispersion attraction. As a result, the core region of the adsorbate is strongly repelled to the O=C-O-C=O functional groups, compare to Tables Table 1 and Table 2. The smallest $Ag_{16}(9,4,3)$ substrate model produces only a shallow potential minimum at an erroneously large distance between the adsorbate and the topmost silver layer. On all other substrate clusters, the strength of the oxygen-silver bonds resembles the MP2 results, so that the oxygen atoms occur at similar heights. Nevertheless, even in the end groups, the B3LYP calculation produces pronounced differences to the MP2 reference: The distortion between carboxylic and anhydride oxygens becomes significantly larger, and the C1 atoms between them are pulled up by the overlap repulsion between naphthalene core and substrate. The minimization of the overlap repulsion requires an increased distance between the molecular core and substrate surface, generating in turn a substantial energetic cost for the internal strain in the bent geometry.

The adsorption geometries obtained with DFT and MP2 on the same model clusters show substantial discrepancies. First, in B3LYP, the average height of NTCDA above the topmost ML Table 3: Upper: Total energy of NTCDA on different Ag clusters, in the optimized geometries obtained with MP2 or B3LYP, without BSSE-CP correction. The total MP2 energy E_{MP2} is de- composed of the Hartree-Fock contribution E_{HF} and the correlation energy E^{corr} . Lower: BSSE- CP corrected energies in the geometry corresponding to the potential minimum when moving the optimized adsorbate geometry rigidly along the distance toward the substrate cluster.

MP2

optimized geometry	E_{MP2}	E_{HF}	E^{corr}_{MP2}	E_{B3LYP}
Ag_{16}(9,4,3)	−2.87	2.05	−4.91	−0.13
Ag_{22}(9,4,9)	−5.33	−0.71	−4.62	−0.98
Ag_{32}(15,16,1)	−4.78	1.86	−6.64	−0.74
Ag_{34}(9,16,9)	−3.85	1.36	−5.22	−2.17
Ag_{50}(15,16,9)				−0.74
BSSE-CP corrected				
Ag_{16}(9,4,3)	−1.00	1.97	−2.97	0.13
Ag_{22}(9,4,9)	−2.45	−0.97	−1.48	−0.35
Ag_{32}(15,16,1)	−1.52	1.64	−3.16	−0.29
Ag_{34}(9,16,9)	−0.45	1.17	−1.62	−0.52
Ag_{50}(15,16,9)				0.05

of the substrate is much larger than in MP2. For the largest Ag_{34}(9,16,9) cluster we can handle with both methods, on average B3LYP places the C atoms at a height of 2.88 Å, significantly above the respective value of 2.57 Å obtained with MP2. Second, the adsorption geometry obtained with DFT is strongly bent, a phenomenon occurring not just along the long axis to reduce the energetic impact of the overlap repulsion involving atoms in the naphthalene core, but also along the short axis: All hydrogens are repelled more than the carbon atom they are attached to. From the comparison of the substrate models Ag_{34}(9,16,9) and Ag_{50}(15,16,9), it is clear that the repulsion of the hydrogen atoms cannot be related to the edge of the substrate cluster: Both substrate models result in the same height difference of 0.15 Å between H atoms and adjacent C atoms.

In sharp contrast to these DFT results, in the MP2 geometry, the overlap repulsion is counterbalanced by attractive dispersion interactions, resulting eventually in a nearly flat adsorbate geometry. Hence, the inclusion of dispersion interactions like in MP2 is a mandatory ingredient for avoiding an adsorbate geometry where a bent molecular core is pushed to too large distances from the substrate, an artifact also observed in earlier DFT calculations of organic adsorbates on noble metals without including dispersion interactions [37, 50, 51] The range of applicability of DFT can be augmented by including dispersion interactions for each pair of atoms [49, 52]. In the more recent release TURBOMOLE 6.4, these corrections can be added to DFT calculations. As an example, we have applied this approach to the optimization of NTCDA on an Ag_{32}(15,16,1) model cluster, comparing Tables Table 1 and Table 2. The pairwise attractive dispersion interactions reduce the distance between the core region of the adsorbate and the substrate by about 0.06 Å, with a much smaller impact on the position of the functional groups. Overall, the height distortions in Table 2 are reduced to the B3LYP calculation without dispersion corrections. However, the buckling of the adsorbate remains more pronounced than in the MP2 geometry. For the substrate cluster Ag_{32}(15,16,1), it is clear that the short-range overlap repulsion between adsorbate and substrate is already fully developed, whereas the sum over long-range dispersion interactions in the B3LYP+D3 calculations remains incomplete. Hence, it is very likely that a more extended or even periodic substrate model would reduce the adsorption height further, as demonstrated recently for calculations of PTCDA adsorbed to silver [44]. A comparison between MP2 and B3LYP+D3 reveals that the wave function-based method accounts already for a larger fraction of the total dispersion interaction, resulting in a reduced adsorption height.

Adsorption energy

Even though the adsorbate geometries found in MP2 calculations on the larger substrate clusters seem reasonably converged, the respective adsorption energies do not follow any simple trend. This finding indicates that unavoidable boundary effects arising from the finite size of the metal clusters inhibit the definition of converged adsorption energy. Nevertheless, the RIMP2 calculations allow an estimate of the relative influence of Hartree-Fock energy and dispersion interactions on the total energy.

In Table 3, we analyze the Hartree-Fock contribution and the dispersion interaction on different substrate models. For all Ag clusters except Ag_{22}(9,4,9), the Hartree-Fock energy E_{HF} is strongly repulsive in the distance range of interest. After moving to the minimum of the BSSE-CP corrected MP2 potential, this repulsion is slightly reduced, a combined effect of a larger distance towards the substrate and the subtraction of a small but positive BSSE. Interestingly, also for the B3LYP optimized geometries, the Ag_{22}(9,4,9) shows particularly favorable total energy, revealing that this specific cluster has rather different electronic properties than the other substrate models.

The MP2 correlation energy E^{corr} depends mainly on the number of Ag atoms in the topmost layer: Only for the Ag_{32}(15,16,1) cluster with the largest number of Ag atoms at the metal-organic interface, the dispersion contribution to the correlation energy is increased substantially. However, after the BSSE-CP correction, the quite different BSSE occurring for different substrate models spoils the apparent systematic trend observed when the BSSE was still included, so that the total MP2 energy $E_{MP2} = E_{HF} + E^{corr}$ shows no systematic dependence on cluster size, apart from the fact that the interaction of NTCDA with Ag_{22}(9,4,9) remains particularly favorable. As opposed to the small BSSE occurring for the Hartree-Fock energy, the long-range dispersion interaction included in E^{corr} is subject to a substantial BSSE. When combined with the distance shift obtained from the minimum of the CP-corrected PES, the attractive correlation energy is reduced substantially by 1.94 eV on Ag_{16}(9,4,3) up to 3.6 eV on Ag_{34}(9,16,9).

The short-range correlation energy included in B3LYP shows a relatively small BSSE. For all substrate models except for the smallest cluster, the interaction energy at the CP-corrected distance remains attractive, but the resulting binding energy is significantly below a previous estimate of −0.92 eV deduced from an extended substrate model [37]. Due to the short-range nature of exchange and correlation included at the B3LYP level, the scatter of the interaction energy between different substrate models remains much smaller than in the MP2 results, but the complete lack of dispersion interactions in B3LYP generates unreliable bent adsorbate geometries.

Bonding mechanism

The chemical interactions involved in the adsorption of NTCDA on Ag(110) can be better understood from a careful investigation of the molecular orbitals (MOs) involved. Although the adsorption geometry obtained with MP2 should be more reliable than the respective B3LYP result, MP2 is not able to provide reasonable MOs since the electronic eigenstates are simply obtained from a Hartree- Fock calculation. Therefore, for an analysis of a given geometry, the short-range correlations included in DFT should improve the reliability of the MOs obtained. In the following, we shall use the adsorption geometry obtained at the MP2 level, but the discussion of electronic orbitals will be based on the B3LYP functional. Scanning the relaxed MP2 geometry of NTCDA along different heights above the substrate, we can investigate the dependence of the orbital energies along that coordinate.

Figure 5 shows the energies of the 50 highest occupied MOs of NTCDA/Ag_{32}(15,16,1) calculated with B3LYP/def-SV(P) as a function of height, defined to the geometry optimized at the MP2/def-SV(P) level. Most eigenstates resemble MOs of the free molecule or the free metal cluster, but their energies have a different slope as a function of the distance between adsorbate and substrate: The energy of molecular states increases with distance, but the energy of metallic states decreases with distance. Both slopes arise from the surprising fact that the charge of the molecule becomes more negative with increasing distance. The reason for this counterintuitive distance dependence is the breaking of Ag-O bonds: The O atoms donate electronic charge into the substrate so that the large negative excess charge coming from the double occupancy of the former molecular LUMO is strongly reduced. For the intermediate distance range shown, this doubly occupied LUMO remains below the Fermi energy of the entire system, but at a much larger distance, eventually, the electronic configuration with neutral subunits becomes more favorable, so that the LUMO of NTCDA will be emptied again.

The well-known cushion effect arising from the overlap between molecular orbitals and substate orbitals reduces the tails of metal states extending into the vacuum, defining, in turn, a substantial contribution to the change of the vacuum level.

Relatively few orbitals are strongly hybridized between adsorbate and substrate, including in particular the ones responsible for the chemical interaction between the carboxylic oxygens and the topmost metal layer. As discussed previously for PTCDA adsorbed to Ag(110), the former LUMO of the adsorbate is doubly occupied [43, 44], with rather little hybridization with metal orbitals, compare to Figure 5 b and c. The Kohn-Sham energy of the LUMO of free NTCDA molecule is -4.08 eV, significantly below the HOMO of the Ag cluster at -3.87 eV, so that two electrons can be transferred from the metal into the molecular LUMO. Angular resolved photoemission spectroscopy (ARPES) from this state proves unambiguously that the angular dependence of electron emission is compatible with a Fourier transform of the molecular LUMO, plus small additional features arising from the hybridization with substrate states [15].

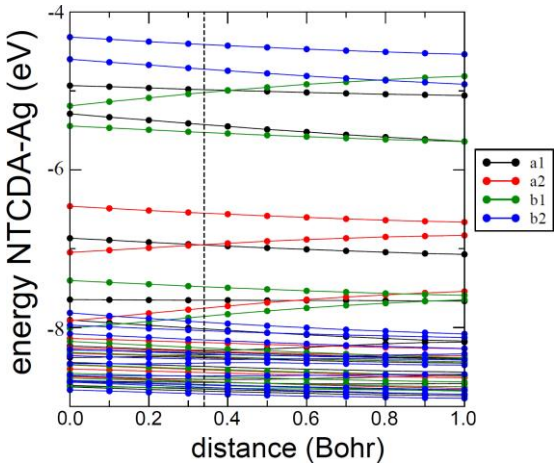

(a)

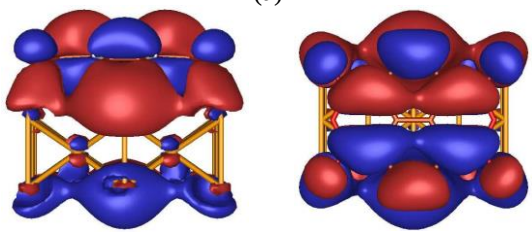

(b) (c)

Figure 14. (a) Scan of B3LYP/SV(P) Kohn-Sham orbital energies for the system NTCDA/Ag22 as a function of the distance between adsorbate and substrate, starting from the relaxed MP2 geometry. The minimum of the CP-corrected MP2 potential is indicated by a vertical

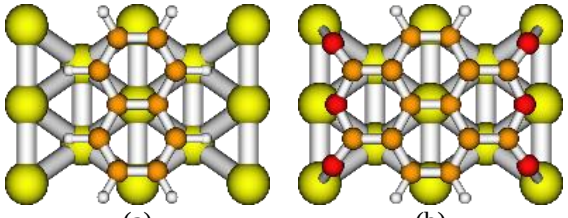

(a) (b)

Figure 15. Top view of naphthalene and NTCDA on Ag22 cluster

Effect of the functional groups on the adsorption geometry

One of the challenging questions arising from the interaction of NTCDA and similar molecules such as PTCDA with the metal surface is which parts (aromatic core or carboxylic groups) have the main effect in the interactions with the surface. NTCDA is a combination of a naphthalene core with two anhydride groups. One way to study the effect of functional groups on the adsorption energy and geometry of NTCDA /Ag(110) is to study the adsorption of naphthalene on the Ag substrate. Here, we put the naphthalene molecule exactly in the position of the naphthalene core in the structure of NTCDA/Ag_{22}, which was obtained from the MP2 calculation (Figure 6). This naphthalene/Ag_{22} structure was optimized using both MP2 and DFT as discussed previously. At the DFT level, the average vertical distance of carbons is 4.48 Å and E_{ads} = 0 eV. These values are 3.23 Å and 1.87 eV at the MP2 level of theory, respectively. These indicate that DFT represents no bonding between naphthalene and Ag(110) whereas MP2 gives strong bonding. On the other hand, the interaction between naphthalene and Ag surface is only vdW interaction which is not included in DFT schemes. We can now find the approximate value of adsorption energy which is due to the anhydride functional group of the NTCDA molecule by subtracting the adsorption energies of NTCDA and naphthalene on the Ag(110) which is 0.57 eV. This value is even larger than the DFT E_{ads} for NTCDA on Ag_{22} (0.35 eV). Therefore, our MP2 calculations demonstrate that the attractive interaction between NTCDA and Ag(110) arises mainly from dispersion interactions between the substrate and naphthalene core. This is in agreement with experimental findings for PTCDA/Ag(110) revealing an attractive interaction between perylene core and silver [16].

Core level shifts

ray photoelectron spectroscopy (XPS) was used to study the binding energy of the 1*s* core levels in carboxylic oxygen O(carb), anhydride oxygen O(anh), and the different carbon sites, both for NTCDA multilayers (thickness 20 MLs) and a single ML on an Ag(111) surface [21, 22]. The experimental and calculated binding energies are summarized in Table 4. The carbon atoms C1 between the oxygen atoms carry a reduced amount of electronic charge, increasing in turn the binding energy of their core levels. For multilayer films, calculated and observed core levels differ by about 6 eV for C atoms and by about 11 eV for O atoms, but after scaling all calculated orbital binding energies by a factor of 1.0235, the deviation reduces to about ±1 eV. Moreover, differences between positively charged C1 sites and essentially neutral carbon atoms in the core region are qualitatively reproduced, and the difference between carboxylic and anhydride oxygens even quantitatively.

In a single adsorbed ML on Ag(111), the negative charge of the adsorbate reduces the binding energies of all core levels [21, 22]. The difference between the carbon core levels on the C1 site and the central naphthalene region was shown to decrease, whereas the difference between the two types of oxygen sites increases [21, 22]. Our calculated core levels deduced from the MP2 geometry of NTCDA adsorbed on the (110)-oriented Ag_{34}(9,16,9) cluster reproduce all of these trends, indicating that changes of the net charges of the various sites show a similar behavior on both substrate orientations.

Conclusion

In this work, we have applied MP2 and DFT calculations to study the adsorption of NTCDA on a (110)-oriented silver surface. To model the adsorbate geometry, we have used rigid Ag clusters of different sizes. Silver clusters consisting of at least 22 atoms gave MP2 adsorbate geometries agreeing within height variations of less than 0.09 Å between different substrate models. Rather strong bonds between carboxylic oxygens and the substrate atoms underneath define the preferential adsorption site and induce specific height variations within the functional groups. In the central naphthalene region, our calculation accounting for a partial compensation between overlap repulsion and attractive dispersion interaction predicts an essentially flat adsorption geometry, whereas the lack of dispersion interaction in DFT results in a bent adsorbate geometry where the central part of the molecule is repelled from the substrate. Dispersion-corrected DFT accounting for pairwise interatomic dispersion potentials still gives a significantly bent adsorbate geometry. From the present results and previous studies of PTCDA adsorbates, we consider wave function-based dispersion interactions included at the MP2 level to be the most adequate approach for investigations of aromatic adsorbates on noble metals

Table 8. Binding energy of the core levels in NTCDA: multilayer, monolayer chemisorbed on Ag(111), and monolayer chemisorbed on Ag(110). All calculations are performed with B3LYP/def-SV(P). The geometry of the free molecule is optimized with B3LYP/def-SV(P), and NTCDA chemisorbed to Ag(110) corresponds to the MP2 geometry on Ag_{34}(9,16,9), scanned to the minimum of the BSSE-CP corrected PES. O1 and O2 represent carboxylic and anhydride oxygens. * Scaled calculated values are obtained using a scaling factor of 1.0235.

	multilayer		Ag(111)		Ag(110)	
	exp.[21]	calc.	scaled*	exp.[22]	calc.	scaled*
C1	289.67	281.92	288.55	286.97	281.21	287.82
C2	286.00	279.21	285.77	284.77	278.20	284.74
C3	285.38	279.31	285.87	284.11	279.00	285.56
C4	285.80	278.95	285.51	283.88	278.46	285.00
O1	532.63	521.42	533.67	530.80	520.96	533.20
O2	534.27	523.03	535.32	533.20	522.86	535.15
C1-C3	4.29	2.61	2.67	2.86	2.21	2.26
C1-C(core)	3.87	2.79	2.86	2.69	2.75	2.81
O(anh)-O(carb)	1.64	1.61	1.65	2.40	1.90	1.94

References

[1] Hung, L. S., & Chen, C. H. (2002). Recent progress of molecular organic electroluminescent materials and devices. Materials Science and Engineering: R: Reports, 39(5-6), 143-222..
https://doi.org/10.1016/S0927-796X(02)00093-1

[2] Dodabalapur, A. (1997). Organic light emitting diodes. Solid state communications, 102(2-3), 259-267.
https://doi.org/10.1016/S0038-1098(96)00714-4

[3] Chen, H., Zhang, W., Li, M., He, G., & Guo, X. (2020). Interface engineering in organic field-effect transistors: principles, applications, and perspectives. Chemical reviews, 120(5), 2879-2949.
https://doi.org/10.1021/acs.chemrev.9b00532

[4] Yan, Y., Zhao, Y., & Liu, Y. (2022). Recent progress in organic field-effect transistor-based integrated circuits. Journal of Polymer Science, 60(3), 311-327.
https://doi.org/10.1002/pol.20210457

[5] Liu, Y., Li, B., Ma, C. Q., Huang, F., Feng, G., Chen, H., ... & Bo, Z. (2022). Recent progress in organic solar cells (Part I material science). Science China Chemistry, 1-45.
https://doi.org/10.1007/s11426-021-1180-6

[6] Mancuso, J. L., Mroz, A. M., Le, K. N., & Hendon, C. H. (2020). Electronic structure modeling of metal–organic frameworks. Chemical reviews, 120(16), 8641-8715..
https://doi.org/10.1021/acs.chemrev.0c00148

[7] Wang, T., Zhang, X., Yuan, N., & Sun, C. (2023). Molecular design of a metal–organic framework material rich in fluorine as an interface layer for high-performance solid-state Li metal batteries. Chemical Engineering Journal, 451, 138819..
https://doi.org/10.1016/j.cej.2022.138819

[8] Okuyama, H., Kuwayama, S., Nakazawa, Y., Hatta, S., & Aruga, T. (2022). Structure and electronic states of strongly interacting metal-organic interfaces: CuPc on Cu (100) and Cu (110). Surface Science, 723, 122126.
https://doi.org/10.1016/j.susc.2022.122126

[9] Dashtian, K., Shahbazi, S., Tayebi, M., & Masoumi, Z. (2021). A review on metal-organic frameworks photoelectrochemistry: A headlight for future applications. Coordination Chemistry Reviews, 445, 214097.
https://doi.org/10.1016/j.ccr.2021.214097

[10] Gerlach, A., Sellner, S., Schreiber, F., Koch, N., & Zegenhagen, J. (2007). Substrate-dependent bonding distances of PTCDA: A comparative x-ray standing-wave study on Cu (111) and Ag (111). Physical Review B, 75(4), 045401..
https://doi.org/10.1103/PhysRevB.75.045401

[11] Henze, S. K. M., Bauer, O., Lee, T. L., Sokolowski, M., & Tautz, F. S. (2007). Vertical bonding distances of PTCDA on Au (1 1 1) and Ag (1 1 1): Relation to the bonding type. Surface Science, 601(6), 1566-1573..
https://doi.org/10.1016/j.susc.2007.01.020

[12] Kröger, I., Stadtmüller, B., Kleimann, C., Rajput, P., & Kumpf, C. (2011). Normal-incidence x-ray standing-wave study of copper phthalocyanine submonolayers on Cu (111) and Au (111). Physical Review B, 83(19), 195414.
https://doi.org/10.1103/PhysRevB.83.195414

[13] Mercurio, G., Bauer, O., Willenbockel, M., Fairley, N., Reckien, W., Schmitz, C. H., ... & Tautz, F. S. (2013). Adsorption height determination of nonequivalent C and O species of PTCDA on Ag (110) using x-ray standing waves. Physical Review B, 87(4), 045421.
https://doi.org/10.1103/PhysRevB.87.045421

[14] Wießner, M., Hauschild, D., Schöll, A., Reinert, F., Feyer, V., Winkler, K., & Krömker, B. (2012). Electronic and geometric structure of the PTCDA/Ag (110) interface probed by angle-resolved photoemission. Physical Review B, 86(4), 045417.
https://doi.org/10.1103/PhysRevB.86.045417

[15] Wießner, M., Kübert, J., Feyer, V., Puschnig, P., Schöll, A., & Reinert, F. (2013). Lateral band formation and hybridization in molecular monolayers: NTCDA on Ag (110) and Cu (100). Physical Review B, 88(7), 075437.
https://doi.org/10.1103/PhysRevB.88.075437

[16] Mercurio, G., Bauer, O., Willenbockel, M., Fiedler, B., Sueyoshi, T., Weiss, C., ... & Tautz, F. S. (2013). Tuning and probing interfacial bonding channels for a functionalized organic molecule by surface modification. Physical Review B, 87(12), 121409.
https://doi.org/10.1103/PhysRevB.87.121409

[17] Stadler, C., Hansen, S., Schöll, A., Lee, T. L., Zegenhagen, J., Kumpf, C., & Umbach, E. (2007). Molecular distortion of NTCDA upon adsorption on Ag (111): a normal incidence x-ray standing wave study. New Journal of Physics, 9(3), 50.
https://doi.org/10.1088/1367-2630/9/3/050

[18] Karl, N., & Günther, C. (1999). Structure and Ordering Principles of Ultrathin Organic Molecular Films on Surfaces of Layered Semiconductors Organic-on-Inorganic MBE. Crystal Research and Technology: Journal of Experimental and Industrial Crystallography, 34(2), 243-254.
https://doi.org/10.1002/(SICI)1521-4079(199902)34:2%3C243::AID-CRAT243%3E3.0.CO;2-5

[19] Schmitz-Hübsch, T., Fritz, T., Sellam, F., Staub, R., & Leo, K. (1997). Epitaxial growth of 3, 4, 9, 10-perylene-tetracarboxylic-dianhydride on Au (111): A STM and RHEED study. Physical Review B, 55(12), 7972.
https://doi.org/10.1103/PhysRevB.55.7972

[20] Glöckler, K., Seidel, C., Soukopp, A., Sokolowski, M., Umbach, E., Böhringer, M., ... & Schneider, W. D. (1998). Highly ordered structures and submolecular scanning tunnelling microscopy contrast of PTCDA and DM-PBDCI monolayers on Ag (111) and Ag (110). Surface science, 405(1), 1-20.
https://doi.org/10.1016/S0039-6028(97)00888-1

[21] Schöll, A., Zou, Y., Jung, M., Schmidt, T., Fink, R., & Umbach, E. (2004). Line shapes and satellites in high-resolution x-ray photoelectron spectra of large π-conjugated organic molecules. The Journal of chemical physics, 121(20), 10260-10267.
https://doi.org/10.1063/1.1807812

[22] Schöll, A., Zou, Y., Schmidt, T., Fink, R., & Umbach, E. (2004). High-resolution photoemission study of different NTCDA monolayers on Ag (111): Bonding and screening influences on the line shapes. The Journal of Physical Chemistry B, 108(38), 14741-14748.

https://doi.org/10.1021/jp049005z
[23] Hauschild, A., Karki, K., Cowie, B. C. C., Rohlfing, M., Tautz, F. S., & Sokolowski, M. (2005). Molecular distortions and chemical bonding of a large π-conjugated molecule on a metal surface. Physical review letters, 94(3), 036106.
https://doi.org/10.1103/PhysRevLett.94.036106
[24] Rurali, R., Lorente, N., & Ordejon, P. (2005). Comment on "molecular distortions and chemical bonding of a large π-conjugated molecule on a metal surface". Physical review letters, 95(20), 209601.
https://doi.org/10.1103/PhysRevLett.95.209601
[25] Hauschild, A., Karki, K., Cowie, B. C. C., Rohlfing, M., Tautz, F. S., & Sokolowski, M. (2005). Hauschild et al. Reply. Physical Review Letters, 95(20), 209602.
https://doi.org/10.1103/PhysRevLett.95.209602
[26] Rohlfing, M., & Bredow, T. (2008). Binding energy of adsorbates on a noble-metal surface: exchange and correlation effects. Physical review letters, 101(26), 266106.
https://doi.org/10.1103/PhysRevLett.101.266106
[27] Sinnokrot, M. O., Valeev, E. F., & Sherrill, C. D. (2002). Estimates of the ab initio limit for π− π interactions: The benzene dimer. Journal of the American Chemical Society, 124(36), 10887-10893.
https://doi.org/10.1021/ja025896h
[28] Sinnokrot, M. O., & Sherrill, C. D. (2006). High-accuracy quantum mechanical studies of π− π interactions in benzene dimers. The Journal of Physical Chemistry A, 110(37), 10656-10668.
https://doi.org/10.1021/jp0610416
[29] Sinnokrot, M. O., & Sherrill, C. D. (2004). Highly accurate coupled cluster potential energy curves for the benzene dimer: sandwich, T-shaped, and parallel-displaced configurations. The Journal of Physical Chemistry A, 108(46), 10200-10207.
https://doi.org/10.1021/jp0469517
[30] Lee, N. K., Park, S., & Kim, S. K. (2002). Ab initio studies on the van der Waals complexes of polycyclic aromatic hydrocarbons. II. Naphthalene dimer and naphthalene–anthracene complex. The Journal of chemical physics, 116(18), 7910-7917.
https://doi.org/10.1063/1.1468642
[31] Gonzalez, C., & Lim, E. C. (2003). Evaluation of the Hartree− Fock dispersion (HFD) model as a practical tool for probing intermolecular potentials of small aromatic clusters: Comparison of the HFD and MP2 intermolecular potentials. The Journal of Physical Chemistry A, 107(47), 10105-10110.
https://doi.org/10.1021/jp030587e
[32] Tsuzuki, S., Honda, K., Uchimaru, T., & Mikami, M. (2004). High-level ab initio computations of structures and interaction energies of naphthalene dimers: Origin of attraction and its directionality. The Journal of chemical physics, 120(2), 647-659.
https://doi.org/10.1063/1.1630953
[33] Boys, S. F., & Bernardi, F. J. M. P. (1970). The calculation of small molecular interactions by the differences of separate total energies. Some procedures with reduced errors. Molecular Physics, 19(4), 553-566.
https://doi.org/10.1080/00268977000101561
[34] Van Duijneveldt, F. B., van Duijneveldt-van de Rijdt, J. G., & van Lenthe, J. H. (1994). State of the art in counterpoise theory. Chemical Reviews, 94(7), 1873-1885.
https://doi.org/10.1021/cr00031a007
[35] Riley, K. E., & Hobza, P. (2007). Assessment of the MP2 method, along with several basis sets, for the computation of interaction energies of biologically relevant hydrogen bonded and dispersion bound complexes. The Journal of Physical Chemistry A, 111(33), 8257-8263.
https://doi.org/10.1021/jp073358r
[36] Jurečka, P., Šponer, J., Černý, J., & Hobza, P. (2006). Benchmark database of accurate (MP2 and CCSD (T) complete basis set limit) interaction energies of small model complexes, DNA base pairs, and amino acid pairs. Physical Chemistry Chemical Physics, 8(17), 1985-1993.
https://doi.org/10.1039/B600027D
[37] Alkauskas, A., Baratoff, A., & Bruder, C. (2006). Site-selective adsorption of naphthalene-tetracarboxylic-dianhydride on Ag (110): First-principles calculations. Physical Review B, 73(16), 165408.
https://doi.org/10.1103/PhysRevB.73.165408
[38] Weigend, F., & Häser, M. (1997). RI-MP2: first derivatives and global consistency. Theoretical Chemistry Accounts, 97, 331-340.
https://doi.org/10.1007/s002140050269
[39] Ahlrichs, R., Bär, M., Häser, M., Horn, H., & Kölmel, C. (1989). Electronic structure calculations on workstation computers: The program system turbomole. Chemical Physics Letters, 162(3), 165-169.
https://doi.org/10.1016/0009-2614(89)85118-8
[40] Andrae, D., Haeussermann, U., Dolg, M., Stoll, H., & Preuss, H. (1990). Energy-adjusted ab initio pseudopotentials for the second and third row transition elements. Theoretica chimica acta, 77, 123-141.
https://doi.org/10.1007/BF01114537
[41] Eichkorn, K., Weigend, F., Treutler, O., & Ahlrichs, R. (1997). Auxiliary basis sets for main row atoms and transition metals and their use to approximate Coulomb potentials. Theoretical Chemistry Accounts, 97, 119-124.
https://doi.org/10.1007/s002140050244
[42] Scholz, R., & Abbasi, A. (2010). Influence of dispersion interactions on the adsorption of PTCDA on Ag (110). physica status solidi c, 7(2), 236-239.
https://doi.org/10.1002/pssc.200982500
[43] Abbasi, A., & Scholz, R. (2009). Ab initio calculation of the dispersion interaction between a polyaromatic molecule and a noble metal substrate: PTCDA on Ag (110). The Journal of Physical Chemistry C, 113(46), 19897-19904.
https://doi.org/10.1021/jp902370b
[44] Bauer, O., Mercurio, G., Willenbockel, M., Reckien, W., Schmitz, C. H., Fiedler, B., ... & Sokolowski, M. (2012). Role of functional groups in surface bonding of planar π-conjugated molecules. Physical Review B, 86(23), 235431.
https://doi.org/10.1103/PhysRevB.86.235431
[45] Pisani, C., Maschio, L., Casassa, S., Halo, M., Schütz, M., & Usvyat, D. (2008). Periodic local MP2 method for the study of electronic correlation in crystals: Theory and preliminary applications. Journal of computational chemistry, 29(13), 2113-2124.

https://doi.org/10.1002/jcc.20975
[46] Erba, A., Casassa, S., Maschio, L., & Pisani, C. (2009). DFT and local-MP2 periodic study of the structure and stability of two proton-ordered polymorphs of ice. The Journal of Physical Chemistry B, 113(8), 2347-2354.
https://doi.org/10.1021/jp809885e
[47] Pisani, C., Schütz, M., Casassa, S., Usvyat, D., Maschio, L., Lorenz, M., & Erba, A. (2012). C ryscor: a program for the post-Hartree–Fock treatment of periodic systems. Physical Chemistry Chemical Physics, 14(21), 7615-7628.
https://doi.org/10.1039/C2CP23927B
[48] Boys, S. F., & Bernardi, F. J. M. P. (1970). The calculation of small molecular interactions by the differences of separate total energies. Some procedures with reduced errors. Molecular Physics, 19(4), 553-566.
https://doi.org/10.1080/00268977000101561
[49] Grimme, S., Antony, J., Ehrlich, S., & Krieg, H. (2010). A consistent and accurate ab initio parametrization of density functional dispersion correction (DFT-D) for the 94 elements H-Pu. The Journal of chemical physics, 132(15), 154104.
https://doi.org/10.1063/1.3382344
[50] Romaner, L., Heimel, G., Brédas, J. L., Gerlach, A., Schreiber, F., Johnson, R. L., ... & Zojer, E. (2007). Impact of bidirectional charge transfer and molecular distortions on the electronic structure of a metal-organic interface. Physical review letters, 99(25), 256801.
https://doi.org/10.1103/PhysRevLett.99.256801
[51] Romaner, L., Nabok, D., Puschnig, P., Zojer, E., & Ambrosch-Draxl, C. (2009). Theoretical study of PTCDA adsorbed on the coinage metal surfaces, Ag (111), Au (111) and Cu (111). New Journal of Physics, 11(5), 053010.
https://doi.org/10.1088/1367-2630/11/5/053010
[52] Grimme, S., Antony, J., Schwabe, T., & Mück-Lichtenfeld, C. (2007). Density functional theory with dispersion corrections for supramolecular structures, aggregates, and complexes of (bio) organic molecules. Organic & Biomolecular Chemistry, 5(5), 741-758.
https://doi.org/10.1039/B615319B